# A defect of the vacuolar putative lipase Atg15 accelerates degradation of lipid droplets through lipolysis.

AUTHOR(S):

Maeda, Yuichiro; Oku, Masahide; Sakai, Yasuyoshi

# A defect of the vacuolar putative lipase Atg15 accelerates degradation of lipid droplets through lipolysis

Yuichiro Maeda[1], Masahide Oku[1], and Yasuyoshi Sakai[1, 2]

[1]Division of Applied Life Sciences, Graduate School of Agriculture and [2]Research Unit for Physiological Chemistry, the Center for the Promotion of Interdisciplinary Education and Research, Kyoto University, Kitashirakawa-Oiwake, Sakyo, Kyoto 606-8502, Japan

To whom correspondence should be addressed: Yasuyoshi Sakai
Division of Applied Life Sciences, Graduate School of Agriculture, Kyoto University, Kitashirakawa-Oiwake, Sakyo, Kyoto 606-8502, Japan
Tel: +81-75-753-6385
Fax: +81-75-753-6454
E-mail: ysakai@kais.kyoto-u.ac.jp

**Key words:**

autophagy, Atg15, lipid droplet, lipolysis, Tgl3, Tgl4, triacylglycerol

**Abbreviations:**

DAG, diacylglycerol; ER, endoplasmic reticulum; FFA, free fatty acid; GFP, green fluorescent protein; LDs, lipid droplets; mCherry, monomeric cherry fluorescent protein; PL, phospholipid; PNPLA2/ATGL, patatin-like phospholipase domain containing 2; SE, sterol ester; TAG, triacylglycerol; WT, wild type

**Abstract**

Lipid droplets (LDs) are the conserved organelles for the deposit of neutral lipids, and function as reservoirs of membrane and energy sources. To date, functional links between autophagy and LD dynamics have not been fully elucidated. Here, we report that a vacuolar putative lipase, Atg15, required for degradation of autophagic bodies, is crucial for the maintenance of LD amount in the yeast *Saccharomyces cerevisiae* in the stationary phase. Mutant analyses revealed that the putative lipase motif and vacuolar localization of Atg15 are important for the maintenance of LD amount. Loss of autophagosome formation by simultaneous deletion of core *ATG* genes cancelled the reduction in the LD amount in *ATG15*-deleted cells, indicating that degradation of autophagic bodies accounts for the functional involvement of Atg15 in LD dynamics. The reduced level of LDs in the mutant strain was dependent on Tgl3 and Tgl4, major lipases for lipolysis in *S. cerevisiae*. An altered phosphorylation status of Tgl3, higher accumulation of Tgl4, and closer associations of Tgl3 and Tgl4 with LDs were detected in the *ATG15*-deleted cells. Furthermore, increased levels of downstream metabolites of lipolysis in the mutant strain strongly suggested enhanced lipolytic activity caused by loss of *ATG15*. Our data provide evidence for a novel link between autophagic flux and LD dynamics integrated with Atg15 activity.

## Introduction

The lipid droplet (LD) functions as a main organelle for storage of neutral lipids such as triacylglycerol (TAG) and sterol ester (SE). These neutral lipids are packed into the core of LD, and the surface of LD is surrounded by a phospholipid monolayer.[1] Although LD had been simply considered as an energy-storage organelle, recent studies, most of which addressed yeast LD dynamics, revealed other functions of LD such as those that supply membrane sources and in maintaining lipid homeostasis.[2-4] Intriguingly, this organelle was found connected with other organelles, such as the endoplasmic reticulum (ER), mitochondria, peroxisomes, vacuoles/lysosomes, and also with autophagosomes, which implies functional associations of LDs with lipid metabolisms in these organelles. [5-7] It is thought that LDs are generated from the ER, where several enzymes with acyltransferase activity (Dga1, Lro1, Are1 and Are2) synthesize neutral lipids, leading to the budding of a nascent LD. [8] In fact, LDs are not formed in an *are1*Δ *are2*Δ *dga1*Δ *lro1*Δ strain. [9, 10]

Degradation of LDs is mainly accomplished by lipases localized on LDs, through a process known as lipolysis. In mammalian cells, 2 types of enzymes function in lipolysis, one termed LIPE/HSL (lipase, hormone-sensitive) controlled by a signaling pathway through cyclic AMP, and PNPLA2/ATGL (patatin-like phospholipase domain containing 2).[11] There are no homologs of LIPE in yeast, where most of the triacylglycerol is degraded by 2 lipases, Tgl3, Tgl4, which are localized on LDs in *S. cerevisiae*.[12, 13] Tgl4 is the functional ortholog of PNPLA2 in yeast, harboring a characteristic patatin domain. Lipolytic activity by Tgl4 plays an important role in supplying membrane sources when quiescent ($G_0$) cells are transferred to fresh medium.[14] Both Tgl3 and Tgl4 possess enzymatic activities in addition to those as triacylglycerol lipases; Tgl3 has acyltransferase activity[15] and Tgl4 exhibits a lipase activity toward SE as well as acyltransferase activity.[16]

Recently, a degradation pathway of LD by autophagy (lipophagy) was discovered.[17] The relationship between autophagy and LD in mammalian cells was originally reported in a study of hepatocytes,[18] and subsequent findings based on electron microscopy confirmed that LDs are surrounded by autophagosomes in mice.[19] In yeast cells, a similar phenomenon (incorporation of LDs into the vacuole) was already reported in 1979.[20] Recently, it was reported that LDs are directly incorporated into the vacuole through a microautophagic pathway, when cells are grown on oleate and then transferred to a nitrogen starvation medium, or when the cells are grown in synthetic complete (SC) medium to stationary phase.[21, 22] This process, termed microlipophagy, was reported to require many *ATG* genes that are needed for macroautophagy. However, to date,

little is known about the functional relationship between LD dynamics and autophagy except for the existence of lipophagy. In this study we carried out a comprehensive analysis of LDs in *atg* mutants, and found that Atg15 is specifically required for the maintenance of LD amount in post-diauxic to stationary phases.

In yeast, vesicles transported into the vacuole through macroautophagy (macroautophagic bodies) are lysed by Atg15, and then the released contents including proteins are degraded mainly by intravacuolar proteases.[23] Atg15 is also essential for the degradation of the cytoplasm to vacuole targeting (Cvt) bodies and multivesicular body vesicles in *S. cerevisiae*.[24-26] In the denoted yeast microlipophagy, Atg15 is required for the vacuolar degradation of the neutral lipids in LDs.[21] In this study, we revealed that Atg15 involvement in the maintenance of LD amount was dependent on the protein's putative lipase motif, and was canceled in multiple *atg* mutants defective in macroautophagy, suggesting that the enzymatic activity of Atg15 toward macroautophagic bodies was critical for the maintenance of LD amount. We further discovered that the Atg15 contribution to LD amount was dependent on the lipolytic enzymes Tgl3 and Tgl4, whose *in vivo* activities were strongly suggested to be elevated by loss of Atg15. Altogether, this study provides a novel insight to autophagic flux and LD dynamics.

## Results

### Deletion of *ATG15* causes a decrease in LD in the stationary phase

To study the effects of autophagy on the dynamics of LD, we carried out the quantification of TAG levels in the set of core *atg* mutants (*atg1*Δ through *atg18*Δ), [27] grown in SC medium for 3 days. We found that the TAG amounts (standardized with the optical density [$OD_{600}$] of the culture) varied depending on the mutant strains. The TAG level was notably higher in *atg2*Δ, *vps30*Δ*/atg6*Δ, and *atg14*Δ cells (**Fig. 1 A**). This result seems to correlate with several lines of data in previous studies: One report analyzing the functions of a mammalian Atg2 homolog showed that this protein localizes on LDs and reduces LD amount,[28] and the other study reported that knockdown of the mammalian Atg14 homolog, a component of the class III phosphatidylinositol 3-kinase complex together with BECN1 (Vps30/Atg6 homolog), elevated TAG levels in liver and serum. [29]

Interestingly, unlike other *atg* mutants, the TAG amount in *atg15*Δ cells was significantly lower than that in its parental wild-type cells (**Fig. 1A**). We also conducted fluorescence microscopy of LDs by staining the organelle with BODIPY 493/503. The number of LDs in the *atg15*Δ strain was comparable to that in the wild-type strain when the cells were grown in SC medium for 12 h to a mid-log growth phase (**Fig. 1B, C and D**). In contrast, the number of LDs was found to be markedly smaller at the post-diauxic phase in the *atg15*Δ cells relative to that in the wild-type cells (**Fig. 1B, C and D**). This drop in the number of LDs in the *atg15*Δ cells was evident throughout the culture period thereafter (**Fig. 1C and D**). In accordance with the microscopy analysis, the amounts of TAG and SE, the main components of LDs, in the *atg15*Δ cells were about half those in the wild-type cells when they were cultured in SC medium for 48 h (**Fig. 1E and F**). We confirmed the induction of autophagy under this culture period by the detection of GFP-Atg8 fluorescence in the vacuole (fluorescence microscopy), as well as the detection of a cleaved band from GFP-Atg8 (immunoblot analysis), in the cells cultured in SC medium for 48 h (**Fig. S1A and B**). In contrast, fluorescence microscopy of the vacuolar membrane (stained with FM 4-64 dye) and LD (stained with BODIPY 493/503) visualized few LDs inside the vacuole of the wild-type and *atg15*Δ cells 48 h after the start of the culture (Fig. S1C). These results demonstrate that Atg15 functions in the maintenance of LD amount in cells in post-diauxic to stationary phases, when autophagic activities, but not the morphological signs of stationary-phase lipophagy,[22] are detected.

### Vacuolar localization and the putative lipase motif of Atg15 are important for the

**maintenance of LD amount**

Fluorescence microscopy observation of cells with GFP-tagged Atg15 showed the diffusion of GFP fluorescence in the vacuole, confirming that Atg15 was accumulated in this compartment (**Fig. 2A**). A previous work showed that Atg15 harbors a GXSXG putative lipase motif which is required for the degradation of autophagic bodies.[25] Additionally, another study reported that when the endogenous Atg15 was replaced by an Atg15 derivative with an HDEL motif (an ER retention/retrieval signal in yeast) at its C terminus, the maturation of precursor Ape1, the main cargo of Cvt vesicles, was diminished. [24] To address whether the putative lipase activity and vacuolar localization of Atg15 are required for its functional involvement in LD dynamics, we expressed in *atg15*Δ cells an Atg15 variant mutated within the putative lipase motif, Atg15$^{S332A}$, or another Atg15 variant fused to the HDEL sequence (Atg15-HDEL). Both the number of LD and TAG level were markedly reduced in the mutants expressing Atg15$^{S332A}$ than in the corresponding wild-type cells when they were cultured in SC medium for 48 h (**Fig. 2B and C**). We confirmed ER localization of Atg15-GFP-HDEL expressed with its native promoter in *atg15*Δ cells under the same culture conditions (data not shown). The LD number and TAG level were also found decreased in the mutant cells with Atg15-HDEL cultured in SC medium for 48 h (**Fig. 2B and C**). Thus, these results indicate that the putative lipase activity of Atg15 in the vacuole is important for the LD maintenance in stationary phase.

**Absence of macroautophagy suppresses the deficiency of LD in *atg15*Δ cells**

Atg15 activity in the vacuole disintegrates multiple types of vesicles including those generated by the multivesicular body pathway and autophagic bodies. In order to investigate whether the involvement of Atg15 in LD dynamics indeed requires autophagic flux, we generated *atg1*Δ *atg15*Δ cells (**Fig. 3A**). The number of LDs and TAG level in *atg1*Δ *atg15*Δ cells after culturing the cells in SC medium for 48 h was found to be comparable to those in wild-type cells (**Fig. 3B and C**), indicating a cancellation of the phenotype of the *ATG15*-deleted strain by the simultaneous deletion of the *ATG1* gene. This suggested that an Atg1-dependent activity is a prerequisite for the Atg15 involvement in LD dynamics. Similar results were obtained for other *atg* mutants defective in macroautophagy, as well as for a *vac8*Δ mutant that exhibits a significant drop in macroautophagic activity (**Fig. 3D**). [30] In contrast, in deletion mutants of *ATG11*, *ATG19*, *ATG21*, or *ATG32*, the genes for selective autophagic pathways,[31-35] the number of LD was decreased by additional disruption of *ATG15* (**Fig. 3D**). These results indicated that the function of Atg15 in LD dynamics is dependent on

macroautophagic flux to the vacuole, but not on selective autophagy.

Next, we investigated whether accumulation of macroautophagic bodies caused by another approach led to the same phenotype as that seen in the *atg15*Δ cells. For this purpose we generated a *pep4*Δ *prb1*Δ strain that is devoid of the main proteases in the vacuole and accumulates macroautophagic bodies. [23] After culture in SC medium for 48 h, this mutant strain exhibited a significant reduction in the amount of TAG and the number of LD in comparison with the wild-type strain, similar to *atg15*Δ cells (**Fig. 3E and F**). Further deletion of the *ATG15* gene in the *pep4*Δ *prb1*Δ strain had no affect on the TAG level and the number of LD (**Fig. 3E and F**), strongly suggesting that the proteases and Atg15 act in the same process, that is, degradation of macroautophagic bodies.

In order to examine whether the LD amount was affected by blockade of the autophagy flux at another step, namely the fusion of autophagosomes with the vacuolar membrane, we generated *ypt7*Δ and *atg15*Δ *ypt7*Δ strains lacking a small GTPase protein that is required for the fusion step.[36] We found that 1) the number of LDs in *ypt7*Δ cells was slightly increased similar to that in the wild-type cells, and unlike the decreased number of LDs seen in the *atg15*Δ strain, and 2) further deletion of the *ATG15* gene in the *ypt7*Δ cells did not cause a remarkable decrease in the number of LDs (**Fig. 3D**). From these data we concluded that the accumulation of autophagic bodies in the vacuole, not that of autophagosomes in the cytoplasm, caused the decrease in the amount of LDs. And the latter result was consistent with our finding that the autophagic flux to the vacuole is a prerequisite of Atg15 involvement in LD dynamics.

**The decrease of LDs in *atg15*Δ cells is dependent on Tgl3 and Tgl4**

For elucidating the molecular mechanism underlying Atg15 function in the maintenance of LD dynamics, we hypothesized 2 possibilities responsible for the reduction of LD: 1) the synthesis of LDs is reduced in *atg15*Δ cells, or 2) the lipolytic activity is augmented in *atg15*Δ cells. To investigate the biosynthetic activity of LDs, we focused on 2 major acyltransferases, Dga1 and Lro1, acting in the final step of TAG synthesis.[37] We generated Dga1-3×HA and Lro1-3×HA to compare the amounts of enzymes in cells in the steady state (48 h after the onset of the culture), but found no detectable differences between the mutant and wild-type cells (**Fig. S2A**). We also generated strains expressing Dga1-mCherry and Lro1-mCherry. Dga1 moves from the ER to LDs to synthesize TAG from DAG in the early stationary phase.[38] In both the wild-type and *atg15*Δ cells, the Dga1-mCherry signal exhibited ring-shaped patterns characteristic of its ER localization, and it was not colocalized with the signal from BODIPY

493/503 representing LD localization, when the cells were cultured in SC medium for 48 h (**Fig. S2B**). In a previous study Lro1 was found localized adjacent to LDs at the diauxic phase.[39] In contrast, fluorescence from Lro1-mCherry in the 48 h-cultured cells was not detected juxtaposed to LDs represented by the BODIPY 493/503 signal (**Fig. S2B**). Based on these observations, the biosynthesis process of LDs was shown to be inactivated both in the wild-type and *atg15*Δ cells under the conditions used for our analysis.

To investigate whether loss of Atg15 caused a reduction in LDs through lipolysis, we generated several mutants lacking the lipolysis enzymes. Fluorescence microscopy of LDs in these mutant strains indicated that while the numbers of the LDs in *tgl3*Δ and/or *tgl4*Δ mutants were comparable to that in the wild-type strain, the sizes of the LDs were augmented in the mutant strains. Notably, fluorescence microscopy with BODIPY 493/503-stained cells showed that the numbers of LDs in *atg15*Δ *tgl3*Δ, *atg15*Δ *tgl4*Δ and *atg15*Δ *tgl3*Δ *tgl4*Δ were similar to that in the *tgl3*Δ, *tgl4*Δ, and *tgl3*Δ *tgl4*Δ strains, respectively (**Fig. 4A and B**). The determination of TAG levels also showed that deletion of *TGL3* and/or *TGL4* cancelled the diminishment of LD abundance caused by disruption of *ATG15* (**Fig. 4B**). Thus, Tgl3 and Tgl4 were found responsible for the degradation of LDs in *atg15*Δ cells.

Next we compared the expression levels of Tgl3 and Tgl4 between the wild-type and *atg15*Δ cells. Immunoblot analysis of Tgl3-3×HA after normal SDS-PAGE showed no differences in the protein amount between wild-type and *atg15*Δ cells at any growth phases (**Fig. 4C**). However, when the cell lysates were applied to Phos-tag SDS-PAGE for better separating the phosphorylated and nonphosphorylated populations of Tgl3-3×HA, we detected only the phosphorylated form (possessing less mobility during the electrophoresis) in the wild-type, and both phosphorylated and nonphosphorylated forms of the protein in the *atg15*Δ samples derived from 18-h and 24-h cultured cells (**Fig. 4D**). Since these time periods corresponded to those when a more remarkable decrease in the LD amount was induced in *atg15*Δ cells (**Fig. 1D**), this result implied that loss of *ATG15* affected the phosphorylation status of Tgl3, leading to further activation of the enzyme.

While the protein abundance of Tgl4-3×HA was found gradually decreased during the culture period in both the wild-type and *atg15*Δ cells, the decline of the Tgl4-3×HA amount was delayed in the *atg15*Δ cells (**Fig. 4C**). Thus, the enhanced degradation of LDs in *atg15*Δ cells correlates with a higher amount of Tgl4 in the mutant than in the wild-type cells, as well as with a different phosphorylation status of Tgl3.

In order to address the localizations of the lipolytic enzymes, we carried out fluorescence

microscopy of Tgl3 and Tgl4 tagged with mCherry after 48 h culture in SC medium (**Fig. 4E**). The signals from Tgl3-mCherry and Tgl4-mCherry were found as grain-like patterns in both wild-type and *atg15*Δ cells, but the colocalization frequencies with LDs (stained with BODIPY 493/503) were significantly higher in the *atg15*Δ cells than in the wild-type cells (**Fig. 4E**). This result showed consistency with the decrease in LD amounts in the *atg15*Δ cells.

**Enhancement of lipolysis affects lipid metabolism in *atg15*Δ cells**

In order to verify the upregulation of lipolytic activity in *atg15*Δ cells, we next carried out quantitative comparisons of metabolites related to mobilization of TAG, between the wild-type and *atg15*Δ cells. As shown in Fig. 5A, *atg15*Δ cells cultured in SC medium for 48 h contained higher levels of diacylglycerol (DAG) than wild-type cells under the same culture conditions. The amount of free fatty acids (FFAs) was also higher in *atg15*Δ cells than in the wild-type cells (**Fig. 5B**).

Next, we speculated that the increase in the products of lipolysis (DAG and FFAs) could lead to enhanced production of phospholipids in the ER. To address this question, we quantified phospholipids in wild-type and *atg15*Δ cells. We found that the cellular phospholipid amount was higher in *atg15*Δ cells than that in wild-type cells (**Fig. 5C**). Since we could not exclude the possibility that the higher level of phospholipid amount in *atg15*Δ cells was caused by accumulation of autophagic bodies inside the vacuole, we also analyzed the phospholipid amount in the microsomal (ER) fraction prepared by subcellular fractionation. The phospholipid amount in the fraction was also higher in *atg15*Δ cells than in wild-type cells (**Fig. 5D**). Additionally, we observed the localization of Opi1, a negative regulator of enzymes for phospholipid synthesis.[40] This protein is localized on the ER when phosphatidic acid is abundantly present in the organelle. Opi1-GFP was observed on ER membrane only in the *atg15*Δ cells, 48 h after culturing in SC medium (**Fig. 5E**). These results indicated that the mobilization of neutral lipids and the synthesis of phospholipids are activated in *atg15*Δ cells.

Finally, we investigated whether the changes in lipid metabolism by loss of Atg15 affected the physiological state of the cells, by comparing cell viabilities of the strains lacking *ATG1*, *ATG15* and/or *TGL3*. While the cell viabilities of all the tested strains were comparable up to 5 days after the start of the culture in SC medium, the *atg15*Δ strain exhibited a more remarkable loss of viability than the wild type or even *atg1*Δ cells, after a prolonged culture for 7 to 9 days (**Fig. 5F**). This result was consistent with a previous study that investigated the cell viability of the *atg15*Δ strain under a nitrogen-starved condition.[26] Of note, the loss of viability found in the

*atg15*Δ strain was partially suppressed by further deletion of the *TGL3* gene (*atg15*Δ *tgl3*Δ; **Fig. 5F**), suggesting that the enhanced lipolysis in the *atg15*Δ strain contributed to the loss of viability of this mutant strain to some extent.

## Discussion

Atg15 was previously identified as the sole putative vacuolar lipase for degradation of autophagic bodies in *S. cerevisiae*.[24,25] To our knowledge, the only functional association of Atg15 with LD metabolism unveiled in *S. cerevisiae* was the enzyme's participation in the final step of lipophagy.[21] This previous study had shown higher accumulation of TAG and lowered lipase activities in the vacuoles of *atg15*Δ cells.[21] In the present work, we revealed that the number of LDs and the amount of neutral lipids were remarkably lower in the *atg15*Δ strain, in comparison to the wild type and the other tested *atg* mutant strains cultured to stationary phase (**Fig. 1**). Results from these 2 studies are not contradictory to each other, since impairment of lipase activities in the vacuole of the mutant may provide a signal resulting in enhancement of lipolytic activity outside the organelle, leading to reduction in the LD amount as a whole. It is also notable that under our culture conditions, we were not able to detect the intravacuole population of LDs reported in a previous report on lipophagy in the stationary phase,[22] in the wild-type nor *atg15*Δ cells (**Fig. S1C**). Since we utilized a different medium from that used in the previous study and observed the LD dynamics at earlier time points (up to 3 days) instead of the observation up to 7 days after the start of the culture in the previous study, the phenotype of the *atg15*Δ strain found in this study was thought to be independent from the outcome of lipophagy in the stationary phase.

Our findings uncovered the putative lipase's important role in the degradation of macroautophagic bodies in the stationary phase, as the phenotype of the *atg15*Δ cells was suppressed by the simultaneous deletion of *ATG* genes required for macroautophagy (**Fig. 3**). The failure to degrade macroautophagic bodies is thought to cause pleiotropic effects on the cell status. The most plausible consequence from this failure is deficiencies of compounds for the biosynthesis of cellular components, due to lack of recycling flow from the vacuole. Another possibility is that the remnant autophagic bodies inside the vacuoles of the mutant cells alter the intravacuolar environments, rendering the cells exposed to more stresses. Indeed, we detected a higher ROS accumulation in *atg15*Δ cells than in the wild-type cells grown to stationary phase (data not shown). These outcomes may cause signaling events to enhance lipolytic activities as discussed below.

Atg15 function in LD dynamics was investigated from the viewpoints of biosynthesis and degradation of the organelle. We could not detect any active populations of the TAG-synthesizing enzymes (Dga1 and Lro1) under our culture conditions, or any differences in protein abundance and localization of these enzymes between the wild-type and *atg15*Δ cells

(**Fig. S2**). In contrast, deletion of genes for lipolysis, *TGL3* and/or *TGL4*, suppressed the reduction in LD and TAG amount in *atg15*Δ cells (**Fig. 4A and 4B**). Although the abundance of Tgl3 was found constant during the culturing to stationary phase and no difference in the amount of the enzyme was detected between the wild-type and *atg15*Δ cells (**Fig. 4C**), the phosphorylation status and localization of the protein were affected by loss of Atg15: in the *atg15*Δ strain, a nonphosphorylated population of the enzyme was detected, but not in the wild-type cells, and Tgl3-mCherry was found more closely associated with LDs in *atg15*Δ cells (**Fig. 4D and E**). A pioneering study on Tgl4 identified phosphorylation events leading to activation of the enzyme.[14] A similar regulation may also exist for Tgl3 in the cells cultured to stationary phase, and the detailed mechanism should be addressed in the future.

In contrast to the constant expression of Tgl3, the intracellular amount of Tgl4 declined after the diauxic shift (**Fig. 4C**), and the kinetics of Tgl4 diminishment were found to be slower in *atg15*Δ cells than in the wild-type cells (**Fig. 4C**). In a mammalian experimental system, the amount of PNPLA2 (the ortholog of Tgl4) is regulated by degradation via the ubiquitin-proteasome pathway.[41] Thus, it is possible that yeast Tgl4 is also degraded by the ubiquitin-proteasome pathway, whose activity is downregulated in *atg15*Δ cells after the diauxic phase.

A previous study revealed that mobilization of TAG by lipolysis supported efficient biosynthesis of phospholipids in the ER.[42] Indeed, our data indicated a higher accumulation of phospholipids in the ER of *atg15*Δ cells, concomitant with the enhancement of mobilization of TAG in the mutant (**Fig. 5A through D**). Opi1, a negative regulator of many phospholipid synthesis enzymes that acts by sensing the abundance of phosphatidic acid at the ER,[40] was localized on ER membranes in *atg15*Δ cells, but not in the wild-type cells (**Fig. 5E**), validating the accumulation of the phospholipid in *atg15*Δ cells. While the enhanced accumulation of phospholipids was deemed to be a consequence from the upregulation of lipolysis, we could not exclude the possibility that the other properties of Tgl3 and Tgl4, namely the acyltransferase activities of these enzymes,[15,16] contributed to the elevated levels of phospholipids in *atg15*Δ cells. Such alternations in lipid metabolism by loss of Atg15 may have significant physiological impacts, since *atg15*Δ cells lose their viability during prolonged culture in SC medium more quickly than the wild-type, or even than *atg1*Δ cells, which was partially reversed by the loss of Tgl3 (**Fig. 5F**).

Although the association of Atg15 in lipophagy was recently analyzed,[21] few studies have addressed the relation between general autophagy and lipolysis. Altogether, our data presented

in this study suggested that degradation of autophagic bodies in the vacuole by Atg15 suppresses lipolysis after the diauxic shift. These findings provide novel insight into the regulatory network of lipid metabolism and autophagy.

## Materials and Methods

### Yeast strains, plasmids, and culture conditions

*Saccharomyces cerevisiae* BY4741 (*MATa his3Δ1 leu2Δ0 met15Δ0 ura3Δ0*) was used as the parental wild-type strain. Cells were grown in SC medium containing 0.67% yeast nitrogen base without amino acids (BD, 291940), 2% glucose, and 0.192% (w/v) yeast synthetic drop-out medium supplements without tryptophan (Sigma-Aldrich, Y1876-20G). All the strains and plasmids used in this study are listed in Table S1 and Table S2. The construction of plasmids for expressing Atg15, Atg15$^{S332A}$ or Atg15-HDEL in yeast cells was done as follows: The genomic sequence covering the 5' promoter, open reading frame, and 3'-untranslated regions of *ATG15* was amplified by PCR using primers as follows, forward; 5'-GCGTTCACAGTTCTCATTTACACTGTAC-3', reverse; 5'–GCATCCATTAGTTGATCTAGACCAGAAG-3', then digested with *Xba*I and *Xho*I, and ligated into *Xba*I/*Xho*I-digested pRS316, yielding the pMB100 plasmid. Plasmids for expressing Atg15$^{S332A}$ or Atg15-HDEL were generated by the inverse PCR method using pMB100 as a template, which yielded pMB101 (encoding Atg15$^{S332A}$) and pMB102 (encoding Atg15-HDEL). The plasmid for expression of Atg15-GFP was generated by the gap-repair cloning method:[43] a GFP-coding DNA fragment was amplified by PCR and cotransformed into yeast cells with a gene fragment that was amplified with pMB100 as a template. The resultant plasmid encoding Atg15-GFP (pMB103) was retrieved form the yeast cells. The yeast gene-deletion strains and the strains expressing the epitope-tagged proteins other than Atg15-GFP were obtained from EUROSCARF or generated by a PCR-based transformation method.[44] The construction of the double gene-deletion strain was performed as described previously.[45] Successful gene disruptions were verified by PCR.

The culturing of the cells in SC medium was done at 28°C with a starting $OD_{600}$ = 0.1.

### Lipid extraction and lipid analyses

Two $OD_{600}$ units of the cells grown in SC medium were harvested by centrifugation, washed once with distilled water, resuspended in 280 µL of 50 mM Tris-HCl buffer (pH 7.0), and subjected to glass-bead disruption. Extraction of lipids from the cell lysate was performed by the Bligh and Dyer method with some modifications.[46] Briefly, to the cell lysate obtained after the glass-bead disruption, 1 ml of chloroform/methanol (1:2), 350 µl of chloroform, and 200 µl of distilled water were successively added and mixed. The samples were centrifuged at 1,000 x *g* for 10 min and the organic phase was retrieved and dried. For separations of neutral lipids, the dried samples were dissolved in chloroform/methanol (2:1) and applied to thin layer

chromatography. TAG and SE were separated using silica gel 60 plates (Merck Millipore, 1.05721.0001) and solvent systems of light petroleum:diethyl ether:acetic acid (30:70:2) followed by light petroleum:diethyl ether (49:1).[47] For separations of DAG and FFA, a mixture of chloroform:acetone:acetic acid (90:8:1) was utilized as the solvent system. The separated lipids were visualized by immersing the plates in 10% $CuSO_4$ (w/v) solution containing 10% $H_3PO_4$ (v/v) and by heating them to 120°C for 30 min. The quantifications of the lipid amounts were done by densitometry using ImageJ software (NIH).[48]

Quantifications of total phospholipids were conducted according to the method established by Broekhuyse.[49] Briefly, total cell lipid extracts were applied to 2-dimensional thin layer chromatography using chloroform:methanol:25% ammonia (65:35:5) as the solvent system for the first dimension, and chloroform:acetone:methanol:acetic acid:water (50:20:10:10:5) for the second dimension. The spots for 5 phospholipids (phosphatidic acid, phosphatidylcholine, phosphatidylethanolamine, phosphatidylinositol, and phosphatidylserine) visualized by staining with iodine vapor were scraped off from the plate, and subjected to determinations of phosphorus.

**Fluorescence microscopy**

Cells were stained with BODIPY 493/503 (Invitrogen, D-3922) in the dark for 10 min at room temperature, washed twice with phosphate-buffered saline (137 mM NaCl, 10 mM $Na_2HPO_4$, 2.7 mM KCl, and 1.8 mM $KH_2PO_4$, pH adjusted to 7.0 with HCl), and immediately subjected to microscopy. Fluorescence microscopy was performed using an IX81 inverted microscope (Olympus) equipped with Uplan Apo 100×1.35 oil iris objective lens. A XF104-3 filter set (Omega Optics) was used for acquiring signals from BODIPY 493/503 and GFP, and mCherry was visualized with a 546/512-nm bandpass excitation filter, a 560-nm dichromatic mirror and a 575/640-nm bandpass emission filter (Omega Optics). Images were processed by Adobe Photoshop software.

For determinations of LD numbers, we manually counted the grain-shaped signals from BODIPY 493/503 staining; when we could discern several grain-shaped structures in one chunk of the signal, we counted the chunk as several LDs.

**Immunoblot analyses**

Total cell lysates for the immunoblot analyses were prepared as follows: Briefly, the cells were centrifuged, washed with distilled water, and resuspended in 0.2 M NaOH solution containing 100 mM dithiothreitol (DTT) for 10 min on ice. The samples were mixed with 1/9 volume of trichloroacetic acid (100% w/v), and after an additional incubation for 15 min on ice,

they were subjected to centrifugation at 13,000×*g* for 5 min at 4°C. The pellet fractions were resuspended in acetone and subjected to centrifugation at 13,000×*g* for 5 min at 4°C. The resultant pellet fractions were dried and resuspended in 1×SDS sample buffer (0.1 M Tris-HCl, pH 7.5, 2% SDS [Wako, 191-07145], 10% glycerol, 20 mM DTT, trace amount of bromophenol blue), incubated for 5 min at 60°C, and then boiled for 3 min. After centrifugation at 10,000×*g* for 1 min at room temperature, the supernatant fractions were resolved by SDS-PAGE. To detect phosphorylation-dependent mobility shifts of Tgl3-3×HA, the whole cell extracts were loaded onto 5.5% SDS-PAGE gels containing 20 μM Phos-tag acrylamide (Wako, 304-93521) and 100 μM $MnCl_2$. The proteins separated by SDS-PAGE were transferred to Immobilon P polyvinylidene difluoride membrane (Merck Millipore, IPVH00010) using a Trans-Blot SD semi-dry transfer cell (Bio-Rad, 170-3940JA), and detected with the indicated antibodies: anti-HA antibody (F-7) (Santa Crutz Biotechnology, sc-7392); anti-Act1 antibody (Abcam, ab8224); anti-GFP monoclonal antiserum (Clontech, 632381); anti–mouse IgG conjugated with HRP (MBL, PM009-7).

Chemiluminescence detection was done with the Western Lightning kit (Perkin-Elmer Life Science, NEL105001EA) and the signals were analyzed with Light-Capture II (ATTO, 2104451).

**Cell fractionation**

For the preparation of spheroplasts, cells were harvested by centrifugation at 4,000×*g* for 5 min and washed twice with sterilized water. The cells (0.5 g wet weight/ml) were resuspended in buffer A (Tris-HCl, pH 9.4, 10 mM DTT) and incubated at 30°C for 20 min. Afterwards cells were washed once with 1.2 M sorbitol (Wako, 198-03755) and suspended in buffer B (1.2 M sorbitol, 20 mM phosphate potassium buffer, pH 7.4). Zymolyase-100T (Nacalai Tesque, 07665-55) was added at a concentration of 2 mg/g wet weight of the cells. The suspension was incubated at 30°C with gentle shaking for 60 min. Spheroplasts were collected by centrifugation for 5 min at 1,500×*g,* and washed twice with 1.2 M sorbitol.

For microsome isolation, the spheroplasts were resuspended in buffer C (5 mM MES-KOH, pH 6.0, 0.6 M sorbitol, 1 mM KCl, 0.5 mM EDTA, 1 mM PMSF, and protease inhibitor cocktail [Roche, 11873580001]) and chilled on ice. The spheroplasts were homogenized with a Dounce homogenizer by applying 20 strokes using a tight fitting pistil. After centrifugation at 3,000×*g* for 5 min at 4°C to remove cell debris and nuclei, the supernatant fractions were collected, and homogenized again, and subjected to ultracentrifugation at 27,000×*g* for 15 min at 4°C in a SW41Ti rotor (Beckman). The floating layers were transferred to a new tube, and were

subjected to ultracentrifugation at 40,000×g for 30 min at 4°C in the SW41Ti rotor. The pellet fractions consisting of highly enriched microsomes were collected, resuspended in 100 mM phosphate-potassium buffer (pH 7.9) and reserved at -80°C until use.

**Assessment of cell viability**

The cell viabilities were assayed by staining the cultured cells with phloxine B (Nacalai Tesque, 27514-92) and fluorescence microscopy, as described previously.[50]

**Acknowledgements**

This work was supported by Grant-in-Aid for Scientific Research on Priority Areas 26111511 (to YS) from the Ministry of Education, Culture, Sports, Science and Technology, Japan and by Grant-in-Aid for Young Scientists (B) 26850064 (to MO) from the Japan Society for the Promotion of Science.

**References**

1. Tauchi-Sato K, Ozeki S, Houjou T, Taguchi R, Fujimoto T. The Surface of Lipid Droplets Is a Phospholipid Monolayer with a Unique Fatty Acid Composition. J Biol Chem 2002; 277:44507-12.

2. Gaspar ML, Hofbauer HF, Kohlwein SD, Henry SA. Coordination of storage lipid synthesis and membrane biogenesis: evidence for cross-talk between triacylglycerol metabolism and phosphatidylinositol synthesis. J Biol Chem 2011; 286:1696-708.

3. Horvath SE, Wagner A, Steyrer E, Daum G. Metabolic link between phosphatidylethanolamine and triacylglycerol metabolism in the yeast Saccharomyces cerevisiae. Biochim Biophys Acta 2011; 1811:1030-7.

4. Zanghellini J, Natter K, Jungreuthmayer C, Thalhammer A, Kurat CF, Gogg-Fassolter G, Kohlwein SD, von Grünberg H-H. Quantitative modeling of triacylglycerol homeostasis in yeast--metabolic requirement for lipolysis to promote membrane lipid synthesis and cellular growth. FEBS J 2008; 275:5552-63.

5. Binns D, Januszewski T, Chen Y, Hill J, Markin VS, Zhao Y, Gilpin C, Chapman KD, Anderson RGW, Goodman JM. An intimate collaboration between peroxisomes and lipid bodies. J Cell Biol 2006; 173:719-31.

6. Goodman JM. The Gregarious Lipid Droplet. J Biol Chem 2008; 283:28005-9.

7. Pfisterer SG, Bakula D, Cezanne A, Robenek H, Proikas-Cezanne T. WIPI beta-propellers at the crossroads of autophagosome and lipid droplet dynamics. Biochem Soc Trans 2014; 42:1414-7.

8. Kassan A, Herms A, Fernández-Vidal A, Bosch M, Schieber NL, Reddy BJN, Fajardo A, Gelabert-Baldrich M, Tebar F, Enrich C, et al. Acyl-CoA synthetase 3 promotes lipid droplet biogenesis in ER microdomains. J Cell Biol 2013; 203:985-1001.

9.Sandager L, Gustavsson MH, Ståhl U, Dahlqvist A, Wiberg E, Banas A, Lenman M, Ronne H, Stymne S. Storage lipid synthesis is non-essential in yeast. J Biol Chem 2002; 277:6478-82.

10. Walther TC, Farese RV. The life of lipid droplets. Biochim Biophys Acta 2009; 1791:459-66.

11. Lafontan M, Langin D. Lipolysis and lipid mobilization in human adipose tissue. Prog Lipid Res 2009; 48:275-97.

12. Athenstaedt K, Daum G. YMR313c/TGL3 encodes a novel triacylglycerol lipase located in lipid particles of Saccharomyces cerevisiae. J Biol Chem 2003; 278:23317-23.

13. Athenstaedt K, Daum G. Tgl4p and Tgl5p, two triacylglycerol lipases of the yeast

Saccharomyces cerevisiae are localized to lipid particles. J Biol Chem 2005; 280:37301-9.

14. Kurat CF, Wolinski H, Petschnigg J, Kaluarachchi S, Andrews B, Natter K, Kohlwein SD. Cdk1/Cdc28-dependent activation of the major triacylglycerol lipase Tgl4 in yeast links lipolysis to cell-cycle progression. Mol Cell 2009; 33:53-63.

15. Rajakumari S, Daum G. Janus-faced enzymes yeast Tgl3p and Tgl5p catalyze lipase and acyltransferase reactions. Mol Biol Cell 2010; 21:501-10.

16. Rajakumari S, Daum G. Multiple functions as lipase, steryl ester hydrolase, phospholipase, and acyltransferase of Tgl4p from the yeast Saccharomyces cerevisiae. J Biol Chem 2010; 285:15769-76.

17. Dong H, Czaja MJ. Regulation of lipid droplets by autophagy. Trends Endocrinol Metab 2011; 22:234-40.

18. Singh R, Kaushik S, Wang Y, Xiang Y, Novak I, Komatsu M, Tanaka K, Cuervo AM, Czaja MJ. Autophagy regulates lipid metabolism. Nature 2009; 458:1131-5.

19. Singh R, Xiang Y, Wang Y, Baikati K, Cuervo AM, Luu YK, Tang Y, Pessin JE, Schwartz GJ, Czaja MJ. Autophagy regulates adipose mass and differentiation in mice. J Clin Invest 2009; 119:3329-39.

20. Moeller CH, Thomson WW. Uptake of lipid bodies by the yeast vacuole involving areas of the tonoplast depleted of intramembranous particles. J Ultrastruct Res 1979; 68:38-45.

21. van Zutphen T, Todde V, de Boer R, Kreim M, Hofbauer HF, Wolinski H, Veenhuis M, van der Klei IJ, Kohlwein SD. Lipid droplet autophagy in the yeast Saccharomyces cerevisiae. Mol Biol Cell 2014; 25:290-301.

22. Wang C-W, Miao Y-H, Chang Y-S. A sterol-enriched vacuolar microdomain mediates stationary phase lipophagy in budding yeast. J Cell Biol 2014; 206:357-66.

23. Takeshige K, Baba M, Tsuboi S, Noda T, Ohsumi Y. Autophagy in yeast demonstrated with proteinase-deficient mutants and conditions for its induction. J Cell Biol 1992; 119:301-11.

24. Epple UD, Eskelinen E-L, Thumm M. Intravacuolar membrane lysis in Saccharomyces cerevisiae. Does vacuolar targeting of Cvt17/Aut5p affect its function? J Biol Chem 2003; 278:7810-21.

25. Epple UD, Suriapranata I, Eskelinen E-L, Thumm M. Aut5/Cvt17p, a Putative Lipase Essential for Disintegration of Autophagic Bodies inside the Vacuole. J Bacteriol 2001; 183:5942-55.

26. Teter SA, Eggerton KP, Scott SV, Kim J, Fischer AM, Klionsky DJ. Degradation of lipid vesicles in the yeast vacuole requires function of Cvt17, a putative lipase. J Biol Chem 2001;

276:2083-7.

27. Mizushima N, Yoshimori T, Ohsumi Y. The role of Atg proteins in autophagosome formation. Annu Rev Cell Dev Biol 2011; 27:107-32.

28. Velikkakath AKG, Nishimura T, Oita E, Ishihara N, Mizushima N. Mammalian Atg2 proteins are essential for autophagosome formation and important for regulation of size and distribution of lipid droplets. Mol Biol Cell 2012; 23:896-909.

29. Xiong X, Tao R, DePinho RA, Dong XC. The autophagy-related gene 14 (Atg14) is regulated by forkhead box O transcription factors and circadian rhythms and plays a critical role in hepatic autophagy and lipid metabolism. J Biol Chem 2012; 287:39107-14.

30. Scott SV, Nice DC, 3rd, Nau JJ, Weisman LS, Kamada Y, Keizer-Gunnink I, Funakoshi T, Veenhuis M, Ohsumi Y, Klionsky DJ. Apg13p and Vac8p are part of a complex of phosphoproteins that are required for cytoplasm to vacuole targeting. J Biol Chem 2000; 275:25840-9.

31. Kanki T, Wang K, Cao Y, Baba M, Klionsky DJ. Atg32 is a mitochondrial protein that confers selectivity during mitophagy. Dev Cell 2009; 17:98-109.

32. Kim J, Kamada Y, Stromhaug PE, Guan J, Hefner-Gravink A, Baba M, Scott SV, Ohsumi Y, Dunn WA, Klionsky DJ. Cvt9/Gsa9 functions in sequestering selective cytosolic cargo destined for the vacuole. J Cell Biol 2001; 153:381-96.

33. Okamoto K, Kondo-Okamoto N, Ohsumi Y. Mitochondria-anchored receptor Atg32 mediates degradation of mitochondria via selective autophagy. Dev Cell 2009; 17:87-97.

34. Scott SV, Guan J, Hutchins MU, Kim J, Klionsky DJ. Cvt19 is a receptor for the cytoplasm-to-vacuole targeting pathway. Mol Cell 2001; 7:1131-41.

35. Stromhaug PE, Reggiori F, Guan J, Wang CW, Klionsky DJ. Atg21 is a phosphoinositide binding protein required for efficient lipidation and localization of Atg8 during uptake of aminopeptidase I by selective autophagy. Mol Biol Cell 2004; 15:3553-66.

36. Kirisako T, Baba M, Ishihara N, Miyazawa K, Ohsumi M, Yoshimori T, Noda T, Ohsumi Y. Formation process of autophagosome is traced with Apg8/Aut7p in yeast. J Cell Biol 1999; 147:435-46.

37. Sorger D, Daum G. Synthesis of triacylglycerols by the acyl-coenzyme A:diacyl-glycerol acyltransferase Dga1p in lipid particles of the yeast Saccharomyces cerevisiae. J Bacteriol 2002; 184:519-24.

38. Markgraf DF, Klemm RW, Junker M, Hannibal-Bach HK, Ejsing CS, Rapoport TA. An ER protein functionally couples neutral lipid metabolism on lipid droplets to membrane lipid

synthesis in the ER. Cell Rep 2014; 6:44-55.

39. Wang C-W, Lee S-C. The ubiquitin-like (UBX)-domain-containing protein Ubx2/Ubxd8 regulates lipid droplet homeostasis. J Cell Sci 2012; 125:2930-9.

40. Carman GM, Henry SA. Phosphatidic acid plays a central role in the transcriptional regulation of glycerophospholipid synthesis in Saccharomyces cerevisiae. J Biol Chem 2007; 282:37293-7.

41. Dai Z, Qi W, Li C, Lu J, Mao Y, Yao Y, Li L, Zhang T, Hong H, Li S, et al. Dual regulation of adipose triglyceride lipase by pigment epithelium-derived factor: a novel mechanistic insight into progressive obesity. Mol Cell Endocrinol 2013; 377:123-34.

42. Rajakumari S, Rajasekharan R, Daum G. Triacylglycerol lipolysis is linked to sphingolipid and phospholipid metabolism of the yeast Saccharomyces cerevisiae. Biochim Biophys Acta 2010; 1801:1314-22.

43. Oldenburg KR, Vo KT, Michaelis S, Paddon C. Recombination-mediated PCR-directed plasmid construction in vivo in yeast. Nucleic Acids Res 1997; 25:451-2.

44. Longtine MS, McKenzie A, Demarini DJ, Shah NG, Wach A, Brachat A, Philippsen P, Pringle JR. Additional modules for versatile and economical PCR-based gene deletion and modification in Saccharomyces cerevisiae. Yeast 1998; 14:953-61.

45. Chinen T, Ota Y, Nagumo Y, Masumoto H, Usui T. Construction of multidrug-sensitive yeast with high sporulation efficiency. Biosci Biotechnol Biochem 2011; 75:1588-93.

46. Bligh EG, Dyer WJ. A rapid method of total lipid extraction and purification. Can J Biochem Physiol 1959; 37:911-7.

47. Leber R, Zinser E, Zellnig G, Paltauf F, Daum G. Characterization of lipid particles of the yeast, Saccharomyces cerevisiae. Yeast 1994; 10:1421-8.

48. Girish V, Vijayalakshmi A. Affordable image analysis using NIH Image/ImageJ. Indian J Cancer 2004; 41.

49. Broekhuyse RM. Phospholipids in tissues of the eye. I. Isolation, characterization and quantitative analysis by two-dimensional thin-layer chromatography of diacyl and vinyl-ether phospholipids. Biochim Biophys Acta 1968; 152:307-15.

50. Noda T. Viability assays to monitor yeast autophagy. Methods in enzymology 2008; 451:27-32.

**Figure legends**

**Figure 1.** Decreases in the amounts of LDs and neutral lipids by loss of Atg15 evident in the cells in post-diauxic to stationary phases. (**A**) Relative TAG amounts in *ATG* gene-deletion mutants. Cells were harvested after growth in SC medium for 72 h, and the total lipids were extracted for determination of TAG amount. The TAG amount was standardized with the optical density ($OD_{600}$) of the culture, and the percentages of the value relative to that of the wild-type strain were presented. Three independent experiments were plotted as mean ± SD. (**B**) Representative growth curves of wild-type (●) and *atg15*Δ (○) cells grown in SC medium. (**C**) LDs in the wild-type and *atg15*Δ cells grown in SC medium for the indicated time periods were stained with BODIPY493/503 for fluorescence microscopy. The corresponding lightfield (DIC) images are also shown. Scale bar: 5 µm. (**D**) Quantifications of LD numbers per cell in the wild type (●) or *atg15*Δ (○) strain during culturing in SC medium. Values represent means ± SD. At least 100 cells were used for the calculation. (**E**) Comparison of TAG levels in the wild-type and *atg15*Δ cells grown in SC medium for 48 h. Three independent experiments were plotted as mean ± SD. The asterisk indicates that the difference between the mutant and wild-type cells is statistically significant ($p$-value < 0.01). (**F**) Comparison of SE levels in the wild-type and *atg15*Δ cells grown in SC medium for 48 h. Three independent experiments were plotted as mean ± SD. The asterisk indicates a $p$-value < 0.01.

**Figure 2.** Enzymatic activity and vacuolar localization of Atg15 are required for the maintenance of LD dynamics. (**A**) *ATG15*-deleted cells co-expressing GFP-tagged Atg15 and Vph1 tagged with mCherry (a vacuole marker) under their own promoter regulations were grown in SC medium for 48 h. The cells were harvested and subjected to fluorescence microscopy. The merged image consists of a green image representing the GFP signal and a red image for the mCherry signal. The corresponding lightfield (DIC) image is also shown. Scale bar: 5 µm. (**B**) Visualization of LDs in *atg15* mutants by fluorescence microscopy. LDs were stained with BODIPY 493/503 after the cells were grown in SC medium for 48 h. Vector means the backbone plasmid for the expression of Atg15 variants (pRS316). The corresponding lightfield (DIC) images are also shown. Scale bar: 5 µm. (**C**) (Left columns) The relative amounts of TAG in the denoted strains after 48 h culture in SC medium were determined and shown so that the TAG level in the wild-type strain was presented as 100% and other values were normalized. The error bars indicate SD values. (Right columns) The numbers of LDs in the cells shown in (**B**) were counted and presented with SD values. At least 100 cells were used

for the calculation. Statistical significance of the differences relative to the values of the *atg15*Δ strain harboring the vector was shown with asterisks ($p < 0.01$) and dagger symbols ($p < 0.05$).

**Figure 3.** Effects of simultaneous disruptions of autophagy-related genes on LD abundance in the *atg15*Δ strain. (**A**) Schematic drawing of autophagosomes, autophagic bodies, and Atg15 in the denoted strains. (**B**) Fluorescence microscopy of LDs stained with BODIPY493/503 in the designated strains after culturing in SC medium for 48 h. The corresponding lightfield (DIC) images are also shown. Scale bar: 5 µm. (**C**) (Left columns) The relative amounts of TAG in the denoted strains after 48 h culture in SC medium were determined and shown so that the TAG level in the wild-type strain was presented as 100%. The error bars indicate SD values. (Right columns) The numbers of LDs in the cells shown in (B) were presented with SD values. At least 100 cells were used for the calculation. The asterisk and dagger symbols indicate *p*-values < 0.05, and the double asterisk indicates a *p*-value < 0.005, in comparison with the values of the *atg15*Δ strain. (**D**) Quantifications of LD numbers in various deletion mutants of autophagy-related genes. The numbers of LDs in the denoted strains cultured in SC medium for 48 h were counted after the staining of LDs with BODIPY493/503 and fluorescence microscopy. The error bars show SD values. At least 100 cells were used for the calculation. (**E**) Fluorescence microscopy of LDs in the denoted mutant strains stained with BODIPY 493/503 after culturing in SC medium for 48 h. The corresponding lightfield (DIC) images are also shown. Scale bar: 5 µm. (**F**) (Left columns) The relative amounts of TAG in the denoted strains after 48 h culturing in SC medium were determined and shown so that the TAG level in the wild-type strain was presented as 100% and the other values were normalized. The error bars indicate SD values. (Right columns) The numbers of LDs in the cells were counted and presented with SD values. At least 100 cells were used for the calculation. Statistical significance of the differences was shown with the asterisk and dagger symbols indicating *p*-values < 0.05, and the double asterisk indicating a *p*-value < 0.01.

**Figure 4.** Tgl3 and Tgl4 are responsible for LD reduction in *atg15*Δ cells**.** (**A**) Fluorescence microscopy of LDs in the denoted lipolysis mutant strains stained with BODIPY 493/503 after culturing in SC medium for 48 h. The corresponding lightfield (DIC) images are also shown. Scale bar: 5 µm. (**B**) (Left columns) The relative amounts of TAG in the denoted strains after 48 h culturing in SC medium were determined and shown so that the TAG level in the wild-type strain was presented as 100% and the other values were normalized. (Right columns) The

numbers of LDs in the cells shown in (**A**) were presented with SD values. At least 100 cells were used for the calculation. The asterisk and dagger symbols indicate that the differences of the values in comparison with the wild-type strain are statistically significant ($p < 0.01$) and the double asterisk indicates a $p$-value < 0.01. (**C**) Wild-type and *atg15*Δ cells expressing Tgl3-3×HA and Tgl4-3×HA under their own promoter regulations were cultured in SC medium for the indicated time periods and analyzed by immunoblot analysis with anti-HA and anti-Act1 (beta actin) antibodies. (**D**) Analysis of Tgl3-3×HA phosphorylation status in wild-type and *atg15*Δ cells. Protein extracts acquired after culturing in SC medium for the indicated time periods were separated by SDS-PAGE supplemented with 20 μM Phos-tag acrylamide, and then subjected to immunoblot analysis with anti-HA antibody. (**E**) Localizations of Tgl3-mCherry and Tgl4-mCherry in wild-type and *atg15*Δ cells after 48 h culturing in SC medium are shown along with the LD patterns (stained with BODIPY 493/503). The merged images are composed of green images representing the BODIPY 493/503 signal and red images for the mCherry signal. The corresponding lightfield (DIC) images are also shown. More than 200 dot patterns of the mCherry signal were assessed for their colocalization with the dot patterns of the BODIPY 493/503 signal. The percentage of the mCherry dots showing complete colocalization with, partial association with, or separation from the BODIPY 493/503 dots were presented in the top, middle, and bottom rows in the colocalization sections.

**Figure 5.** Increased levels of DAG, FFAs, and phospholipids in *atg15*Δ cells. (**A**) Quantification of DAG amount in wild-type and *atg15*Δ cells grown in SC medium for 48 h. The values from 3 independent experiments were plotted as mean ± SD. The asterisk indicates that the difference is statistically significant ($p$-value <0.05). (**B**) Quantification of FFA amounts in wild-type and *atg15*Δ cells grown in SC medium for 48 h. The values from 3 independent experiments were plotted as mean ± SD. The asterisk indicates that the difference is statistically significant ($p$-value <0.05). (**C**) Quantification of phospholipid amounts in wild-type and *atg15*Δ cells grown in SC medium for 48 h. The values from 3 independent experiments were plotted as mean ± SD. The double asterisk indicates that the difference is statistically significant ($p$-value <0.005). (**D**) Quantification of phospholipid amounts in microsome fractions of wild-type and *atg15*Δ cells grown in SC medium for 48 h. The values from 3 independent experiments were plotted as mean ± SD. The asterisk indicates that the difference is statistically significant ($p$-value <0.05). (**E**) Wild-type and *atg15*Δ cells expressing Opi1 tagged with GFP under its own promoter regulation were cultured in SC medium for 48 h. Cells were harvested and

subjected to fluorescence microscopy. The GFP images along with the corresponding lightfield (DIC) images are shown. The arrows indicate Opi1-GFP signals exhibiting an ER-localization pattern. Scale bar: 5 µm. (**F**) Cell viabilities of the denoted strains cultured in SC medium for the indicated time periods were calculated by fluorescence microscopy of dead cells stained with phloxine B. The error bars represent SD values.

**Supplemental figure legends**

**Figure S1.** Induction of macroautophagy in cells cultured in SC medium for 48 h. (**A**) Localization of GFP-Atg8 in cells cultured in SC medium for 48 h. GFP-tagged Atg8 and Vph1 (a marker for the vacuolar membrane) tagged with mCherry were expressed under their own promoter regulations in wild-type and *atg1*Δ cells. The cells were cultured in SC medium for 48 h and subjected to fluorescence microscopy. The merge images consist of green images representing the GFP signal and red images for the mCherry signal. Scale bar: 5 μm. (**B**) Wild-type and *atg1*Δ cells expressing GFP-tagged Atg8 under its own promoter regulation were grown in SC medium for 48 h. Total cell lysates were acquired from the cells and were subjected to immunoblot analysis with anti-GFP antibody. (**C**) The denoted strains were cultured in SC medium for 48 h, stained with BODIPY 493/503 (for visualizing LDs) and FM 4-64 (for visualizing the vacuolar membrane), and subjected to fluorescence microscopy. The merged images consist of red FM 4-64 images and green BODIPY 493/503 images. The corresponding lightfield (DIC) images are also shown.

**Figure S2.** Expression levels and localizations of acyltransferases for synthesis of TAG. (**A**) Detection of Dga1-3×HA and Lro1-3×HA in wild-type and *atg15*Δ cells cultured in SC medium for 48 h by immunoblot analysis with anti-HA and anti-Act1 (beta actin) antibodies. (**B**) The wild-type and *atg15*Δ cells expressing Dga1-mCherry or Lro1-mCherry were subjected to fluorescence microscopy, after the cells were grown in SC medium for 48 h and stained with BODIPY 493/503. The merged images were constructed from the mCherry images (red) and the images representing BODIPY 493/503 signals (green). Scale bar: 5 μm.

**Table S1.** Yeast strains used in this study.

| Strain | Genotype | Source |
|---|---|---|
| BY4741 | *MATa leu2Δ0 his3Δ1 ura3Δ0 met15Δ0* | EUROSCARF |
| Laboratory collection | *atg1Δ::KanMX4* BY4741 | EUROSCARF |
| Laboratory collection | *atg2Δ::KanMX4* BY4741 | EUROSCARF |
| Laboratory collection | *atg3Δ::KanMX4* BY4741 | EUROSCARF |
| Laboratory collection | *atg4Δ::KanMX4* BY4741 | EUROSCARF |
| Laboratory collection | *atg5Δ::KanMX4* BY4741 | EUROSCARF |
| Laboratory collection | *vps30Δ/atg6Δ::KanMX4* BY4741 | EUROSCARF |
| Laboratory collection | *atg7Δ::KanMX4* BY4741 | EUROSCARF |
| Laboratory collection | *atg8Δ::KanMX4* BY4741 | EUROSCARF |
| Laboratory collection | *atg9Δ::KanMX4* BY4741 | EUROSCARF |
| Laboratory collection | *atg10Δ::KanMX4* BY4741 | EUROSCARF |
| Laboratory collection | *atg11Δ::KanMX4* BY4741 | EUROSCARF |
| Laboratory collection | *atg12Δ::KanMX4* BY4741 | EUROSCARF |
| Laboratory collection | *atg13Δ::KanMX4* BY4741 | EUROSCARF |
| Laboratory collection | *atg14Δ::KanMX4* BY4741 | EUROSCARF |
| Laboratory collection | *atg15Δ::KanMX4* BY4741 | EUROSCARF |
| Laboratory collection | *atg16Δ::KanMX4* BY4741 | EUROSCARF |
| Laboratory collection | *atg17Δ::KanMX4* BY4741 | EUROSCARF |
| Laboratory collection | *atg18Δ::KanMX4* BY4741 | EUROSCARF |
| YMB1501 | *atg15Δ::KanMX6* BY4741 | EUROSCARF |
| YMB1502 | *atg15Δ::KanMX4 pRS316::URA3* BY4741 | This study |
| YMB1503 | *atg15Δ::KanMX6 ATG15::URA3* BY4741 | This study |
| YMB1504 | *atg15Δ::KanMX4 ATG15(S332A)::URA3* BY4741 | This study |
| YMB1505 | *atg15Δ::KanMX6 ATG15-HDEL::URA3* BY4741 | This study |
| YMB1506 | *atg15Δ0 ATG15-GFP::URA3 VPH1-mCherry::KanMX6* BY4741 | This study |
| YMB1507 | *atg1Δ::KanMX6* BY4741 | This study |
| YMB1508 | *atg1Δ::KanMX6 atg15Δ0* BY4741 | This study |
| YMB1509 | *tgl3Δ:: KanMX6* BY4741 | This study |
| YMB1510 | *tgl4Δ::KanMX6* BY4741 | This study |
| YMB1511 | *tgl3Δ0 tgl4Δ0* BY474 | This study |

**Table S1.** Yeast strains used in this study (continued).

| Strain | Genotype | Source |
|---|---|---|
| YMB1512 | *atg15Δ0 tgl3Δ::KanMX6* BY4741 | This study |
| YMB1513 | *atg15Δ0 tgl4Δ::KanMX6* BY4741 | This study |
| YMB1514 | *atg15Δ::KanMX6 tgl3Δ0 tgl4Δ* BY4741 | This study |
| YMB1515 | *TGL3-3×HA::KanMX6* BY4741 | This study |
| YMB1516 | *atg15Δ0 TGL3-3×HA::KanMX6* BY4741 | This study |
| YMB1517 | *TGL4-3×HA::KanMX6* BY4741 | This study |
| YMB1518 | *atg15Δ0 TGL4-3×HA::KanMX6* BY4741 | This study |
| YMB1519 | *TGL3-mCherry::KanMX6* BY4741 | This study |
| YMB1520 | *atg15Δ0 TGL3-mCherry::KanMX6* BY4741 | This study |
| YMB1521 | *TGL4-mCherry::KanMX6* BY4741 | This study |
| YMB1522 | *atg15Δ0 TGL4-mCherry::KanMX6* BY4741 | This study |
| YMB1523 | *OPI1-GFP::KanMX6* BY4741 | This study |
| YMB1524 | *atg15Δ0 OPI1-GFP::KanMX6* BY4741 | This study |
| YMB1525 | *atg8Δ::GFP-ATG8* BY4741 | This study |
| YMB1526 | *atg1Δ0 atg8Δ::GFP-ATG8* BY4741 | This study |
| YMB1527 | *atg15Δ0 atg1Δ::KanMX6* BY4741 | This study |
| YMB1528 | *atg15Δ0 atg2Δ::KanMX6* BY4741 | This study |
| YMB1529 | *atg15Δ0 atg3Δ::KanMX6* BY4741 | This study |
| YMB1530 | *atg15Δ0 atg4Δ::KanMX6* BY4741 | This study |
| YMB1531 | *atg15Δ0 atg5Δ::KanMX6* BY4741 | This study |
| YMB1532 | *atg15Δ0 vps30Δ/atg6Δ0* BY4741 | This study |
| YMB1533 | *atg15Δ0 atg7Δ::KanMX6* BY4741 | This study |
| YMB1534 | *atg15Δ0 atg8Δ::KanMX6* BY4741 | This study |
| YMB1535 | *atg15Δ0 atg9Δ::KanMX6* BY4741 | This study |
| YMB1536 | *atg15Δ0 atg10Δ::KanMX6* BY4741 | This study |
| YMB1537 | *atg15Δ0 atg11Δ::KanMX6* BY4741 | This study |
| YMB1538 | *atg15Δ0 atg12Δ::KanMX6* BY4741 | This study |
| YMB1539 | *atg15Δ0 atg13Δ::KanMX6* BY4741 | This study |
| YMB1540 | *atg15Δ0 atg14Δ::KanMX6* BY4741 | This study |

| | | |
|---|---|---|
| YMB1541 | *atg15Δ0 atg16Δ::KanMX6* BY4741 | This study |

**Table S1.** Yeast strains used in this study (continued).

| Strain | Genotype | Source |
|---|---|---|
| YMB1542 | *atg15Δ0 atg17Δ::KanMX6* BY4741 | This study |
| YMB1543 | *atg15Δ0 atg18Δ::KanMX6* BY4741 | This study |
| YMB1544 | *atg19Δ::KanMX6* BY4741 | This study |
| YMB1545 | *atg15Δ0 atg19Δ::KanMX6* BY4741 | This study |
| YMB1546 | *atg21Δ::KanMX6* BY4741 | This study |
| YMB1547 | *atg15Δ0 atg21Δ::KanMX6* BY4741 | This study |
| YMB1548 | *atg32Δ::KanMX6* BY4741 | This study |
| YMB1549 | *atg15Δ0 atg32Δ::KanMX6* BY4741 | This study |
| YMB1550 | *vac8Δ::SpHIS5* BY4741 | This study |
| YMB1551 | *atg15Δ0 vac8Δ::SpHIS5* BY4741 | This study |
| YMB1552 | *ypt7Δ::KanMX6* BY4741 | This study |
| YMB1553 | *atg15Δ0 ypt7Δ::KanMX6* BY4741 | This study |
| YMB1554 | *pep4Δ::0 prb1Δ::KanMX6* BY4741 | This study |
| YMB1555 | *atg15Δ0 pep4Δ::0 prb1Δ::KanMX6* BY4741 | This study |
| YMB1556 | *DGA1-mCherry::KanMX6* BY4741 | This study |
| YMB1557 | *atg15Δ0 DGA1-mCherry::KanMX6* BY4741 | This study |
| YMB1558 | *LRO1-mCherry::KanMX6* BY4741 | This study |
| YMB1559 | *atg15Δ0 LRO1-mCherry::KanMX6* BY4741 | This study |

**Table S2.** Plasmids used in this study.

| Plasmid | Description | Reference |
|---|---|---|
| pRS316 | *URA3*-based centromeric plasmid | Sikorski and Hieter (1989) |
| pMB100 | pRS316 *ATG15* | This study |
| pMB101 | pRS316 *ATG15(S332A)* | This study |
| pMB102 | pRS316 *ATG15-HDEL* | This study |
| pMB103 | pRS316 *ATG15-GFP* | This study |

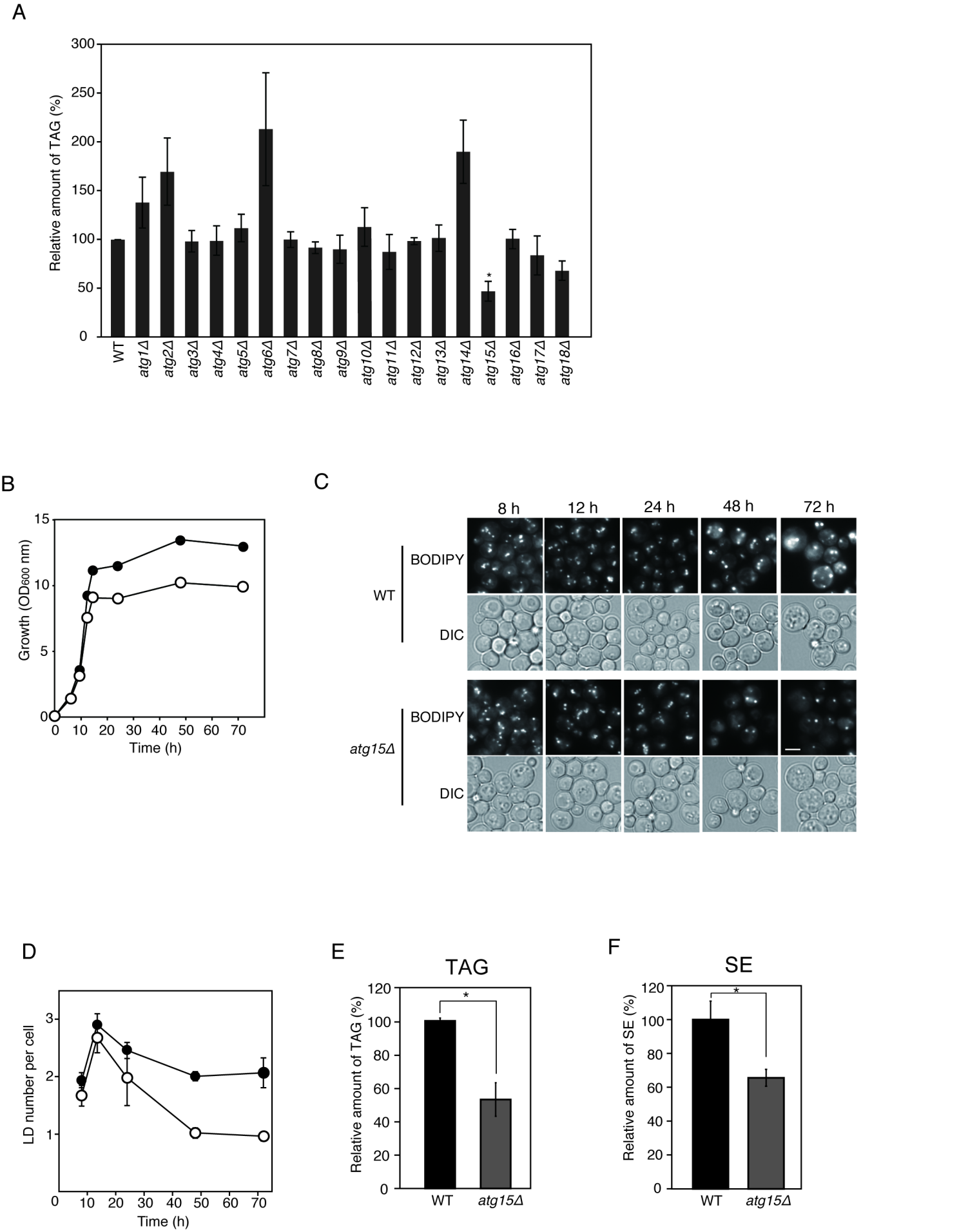

Figure 2

A

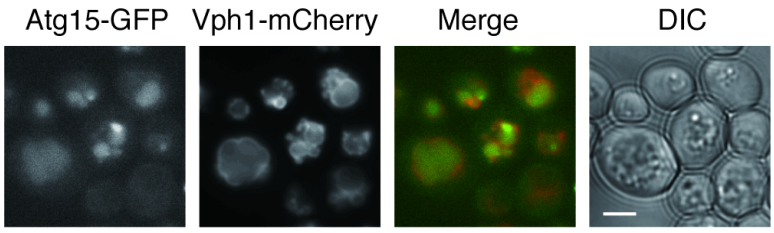


B

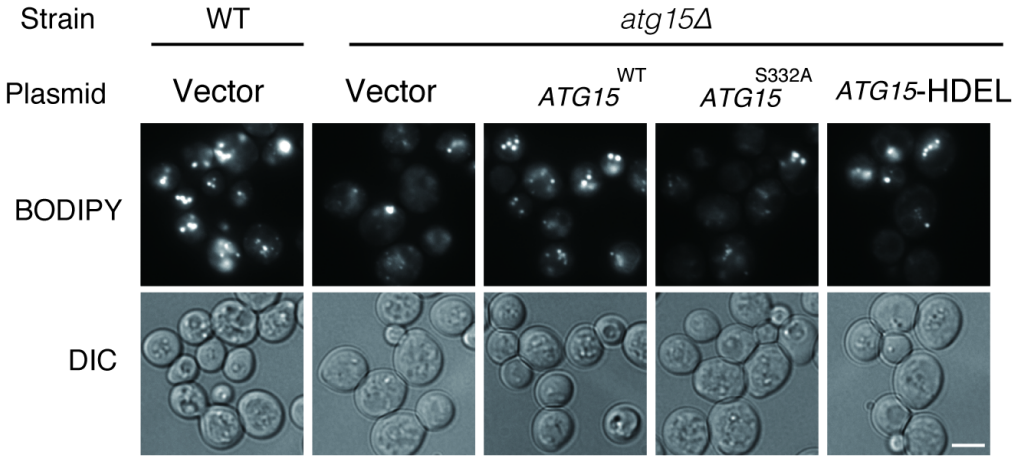


C

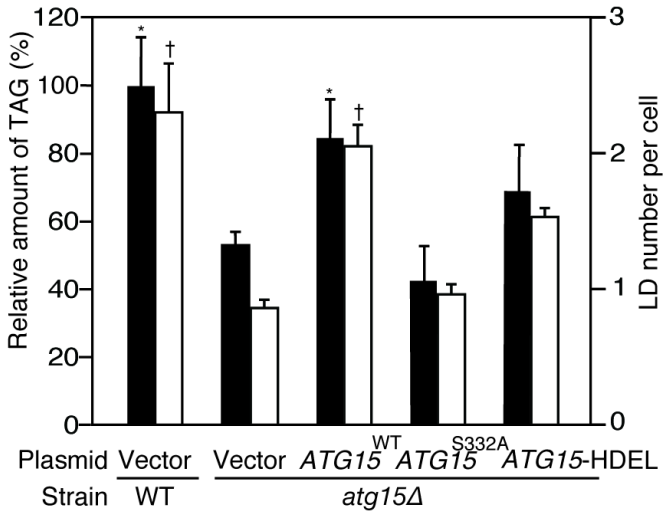

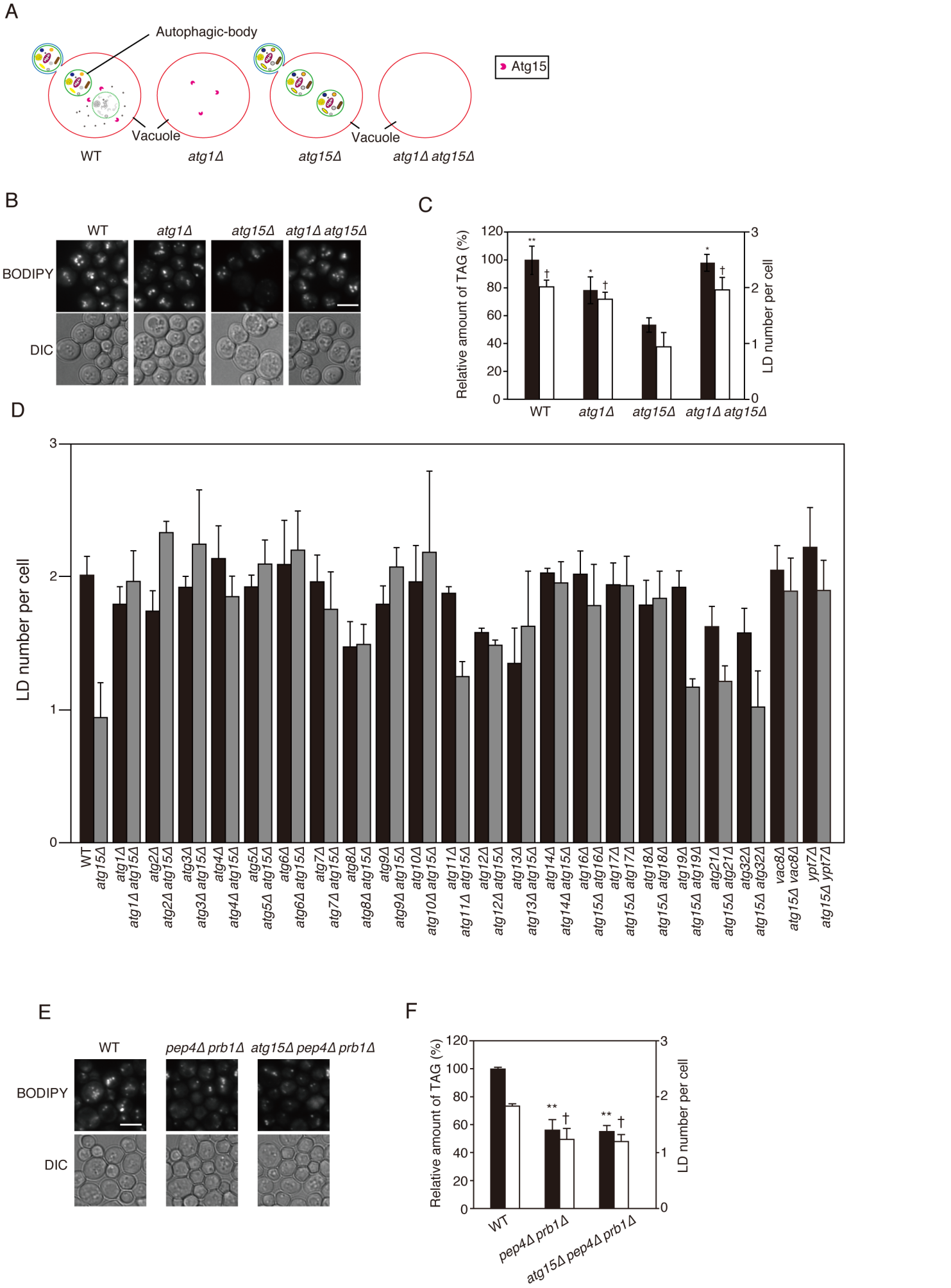

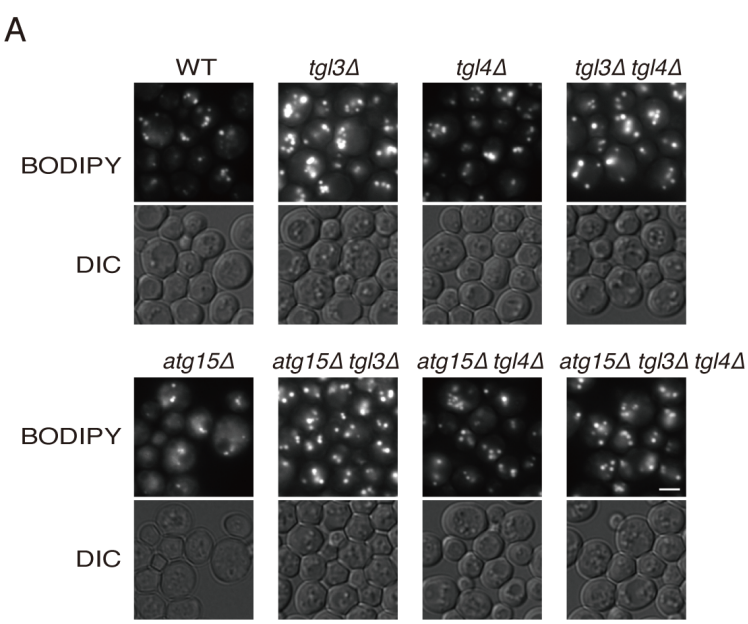


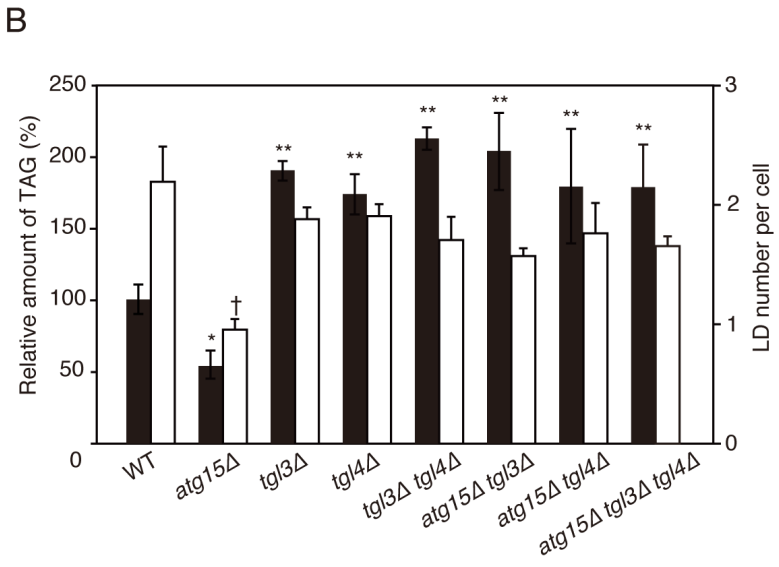


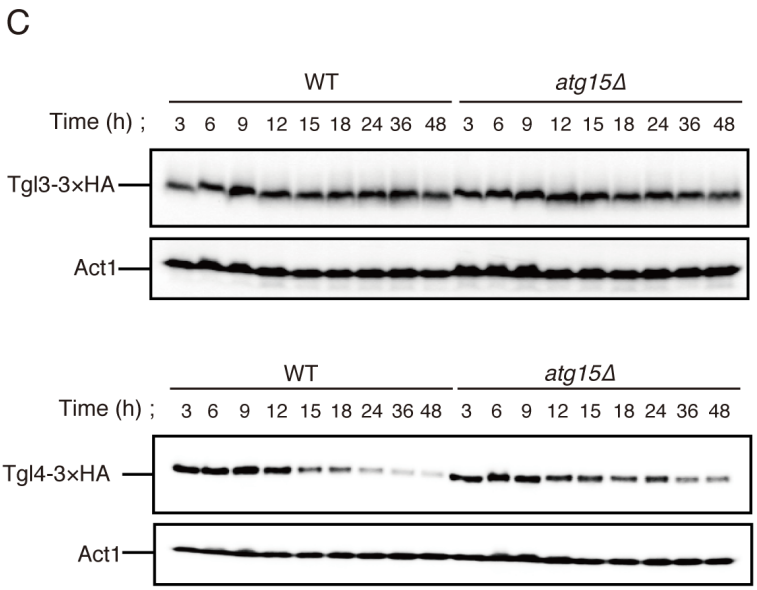


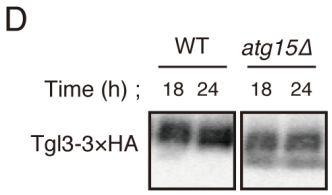


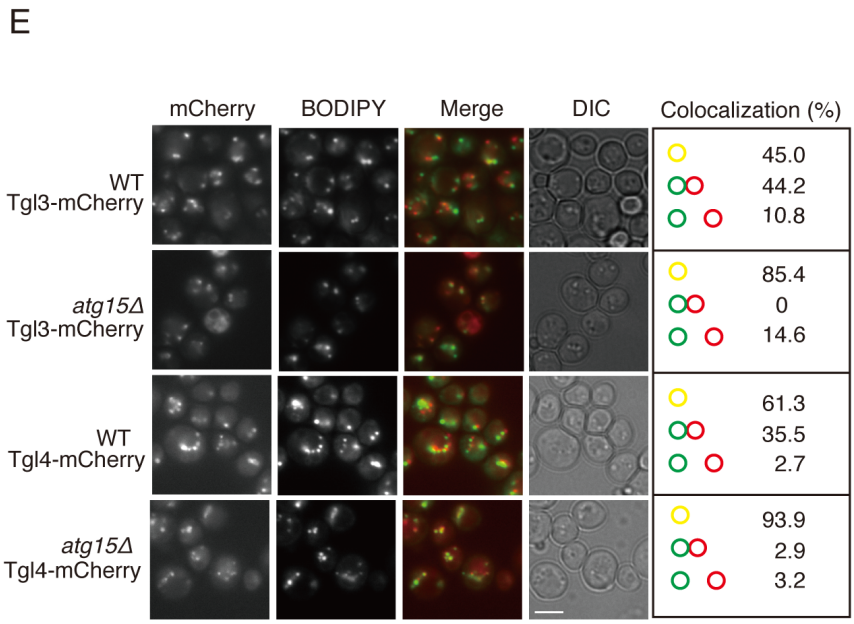

Figure 5

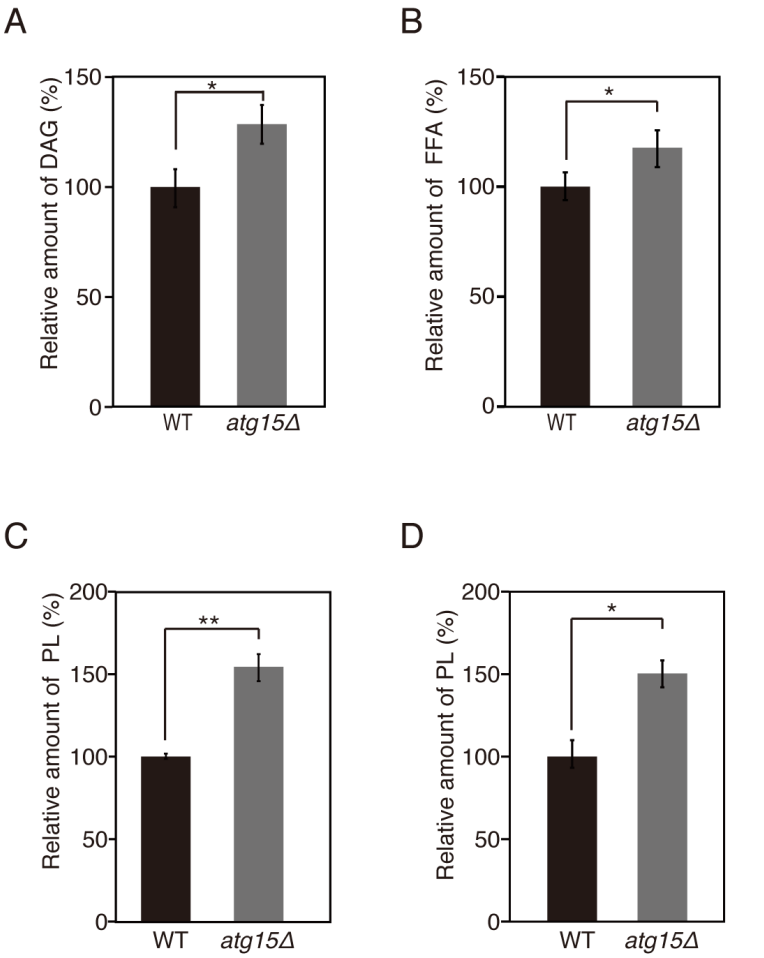


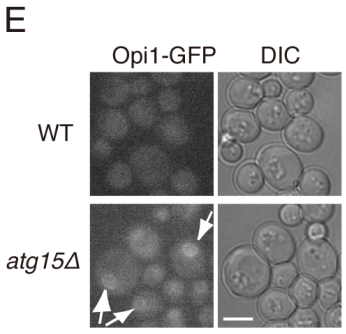


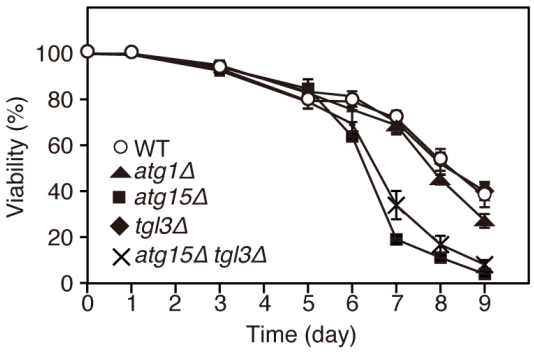

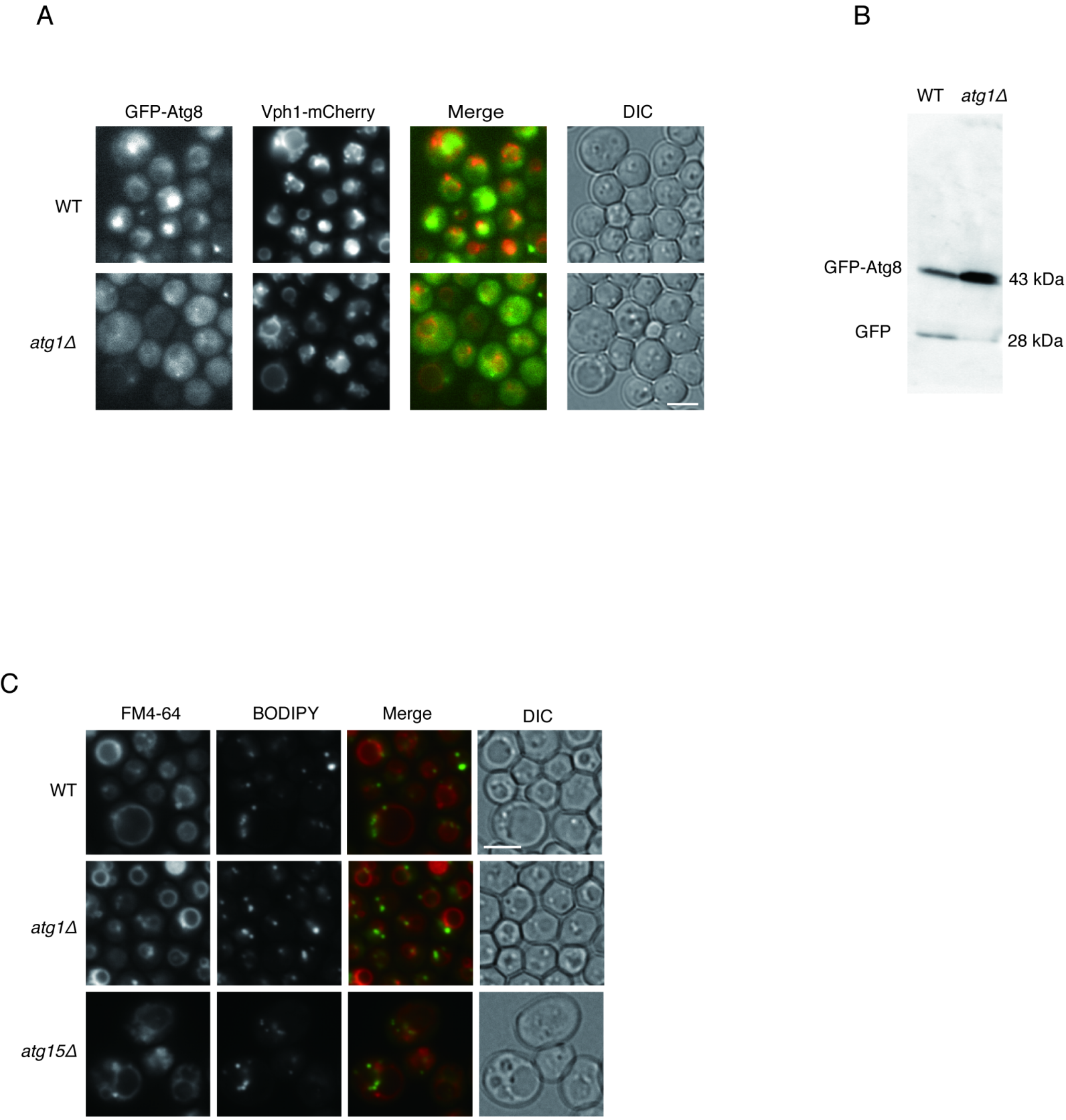

Figure S2